Surface-Enhanced Infrared Absorption: Pushing the Frontier for On-Chip Gas Sensing

Xinyuan Chong,[†] Yujing Zhang,[‡] Erwen Li,[†] Ki-Joong Kim,[§,⊥] Paul R. Ohodnicki,[§,∥] Chih-hung Chang,[‡] and Alan X. Wang*,[†]

[†]School of Electrical Engineering and Computer Science and [‡]School of Chemical, Biological and Environmental Engineering, Oregon State University, Corvallis, Oregon 97331, United States
[§]National Energy Technology Lab, United States Department of Energy, Pittsburgh, Pennsylvania 15236, United States
[∥]Materials Science and Engineering Department, Carnegie Mellon University, Pittsburgh, Pennsylvania 15213, United States
[⊥]AECOM, P.O. Box 618, South Park, Pennsylvania 15216, United States

S Supporting Information

ABSTRACT: Surface-enhanced infrared absorption (SEIRA) is capable of identifying molecular fingerprints by resonant detection of infrared vibrational modes through the coupling with plasmonic modes of metallic nanostructures. However, SEIRA for on-chip gas sensing is still not very successful due to the intrinsically weak light-matter interaction between photons and gas molecules and the technical challenges in accumulating sufficient gas species in the vicinity of the spatially localized enhanced electric field, namely, the "hot-spots", generated through plasmonics. In this paper, we present a suspended silicon nitride (Si_3N_4) nanomembrane device by integrating plasmonic nanopatch gold antennas with metal−organic framework (MOF), which can largely adsorb carbon dioxide (CO_2) through its nanoporous structure. Unlike conventional SEIRA sensing relying on highly localized hot-spots of plasmonic nanoantennas or nanoparticles, the device reported in this paper engineered the coupled surface plasmon polaritons in the metal−Si_3N_4 and metal−MOF interfaces to achieve strong optical field enhancement across the entire MOF film. We successfully demonstrated on-chip gas sensing of CO_2 with more than 1800× enhancement factors by combining the concentration effect from the 2.7 μm MOF thin film and the optical field enhancement of the plasmonic nanopatch antennas.

KEYWORDS: surface-enhanced infrared absorption, plasmonic nanostructure, nanomembrane device, gas sensor, metal−organic framework
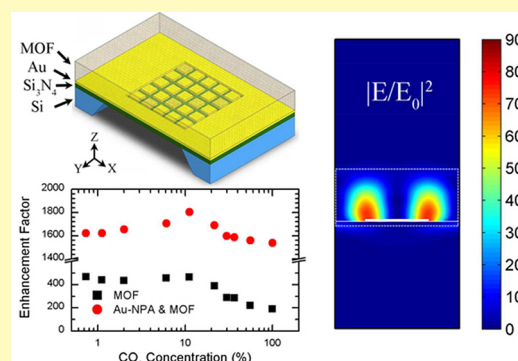
Infrared absorption spectroscopy probes the vibrational modes of various molecular bonds, which can provide structural information on chemical and biological compounds in a label-free manner.[1,2] Infrared absorption is governed by the Beer−Lambert law. Given specific molecules, it requires either a long absorption path or a high density of target molecules to achieve significant infrared absorption. However, for molecules with small infrared absorption cross sections such as gases, or very thin samples such as monolayers, conventional infrared absorption cannot provide good sensitivity. In recent years, on-chip sensors using integrated photonic devices such as the Fabry−Pérot interferometer,[3] ring resonators,[4] photonic crystal slot waveguide,[5] and mid-infrared photonics[6] have been demonstrated due to the enhanced infrared absorption. However, coupling light into waveguide-based integrated photonic devices remains a difficulty for engineering applications.

Surface-enhanced infrared absorption (SEIRA) spectroscopy, which leverages the strong light−matter interaction and subwavelength localization enabled by plasmonic resonances of metallic nanostructures, was first reported by Hartstein et al.[1] and Hatta et al.[7] in the 1980s. Initial studies in SEIRA focused on rough metal surface,[8] metal island films,[9] and metal nanoparticles (NPs).[10] However, the extinction spectra were relatively broad and the plasmonic resonant wavelengths were difficult to control due to the random morphology and distribution of these metallic nanostructures. In recent years, rationally patterned metallic nanostructures with narrow extinction spectra and precisely determined resonant wavelengths due to the dipole-to-dipole interaction, such as nanowire,[11−14] nanoshell,[15] nanosize gap,[16,17] metasurface,[18] nanohole,[19] strip grating,[20] nanodisk,[21] cross-shaped perfect absorber,[22] fan-shaped nanoantennas,[23] nanocrescents,[24] and triangle-shaped nanoantennas,[25] were applied to SEIRA. A thorough review of plasmonic nanostructures for SEIRA was recently published by Neubrech et al.[26] However, existing

applications of SEIRA are exclusively focused on mid-infrared sensing of biomaterials or macromolecules, such as proteins or polymers. SEIRA for gas detection, which is another desirable application for infrared absorption spectroscopy, is not yet very successful due to several intrinsic drawbacks of SEIRA. First, the localized optical field of plasmonic nanostructures limits the light−matter interaction between gas molecules and the optical field. The enhanced infrared absorption can only come from the gas molecules located within the "hot-spots" of plasmonic nanostructures, which usually have very limited volume. Typically, the decay length ($1/e$) of the electric field is within 200−300 nm. Second, the absorption coefficients of gases are intrinsically lower than solid or liquid materials due to the low molecular density. Despite the grand challenges, plasmonics-enhanced gas sensing has been constantly reported in the past years, although not based on the mechanism of SEIRA spectroscopy. Ando et al. reported a device using Au-CuO nanocomposite film for CO sensing.[27] Liu et al. utilized nanoantenna for hydrogen sensing by placing a palladium nanodisk in the nanofocus of a triangular gold nanoantenna.[28] However, existing methods reply on either the change of absorption peak or the spectrum shift, which is indirect sensing with relatively low selectivity.

In our previous work,[29] we demonstrated a prototype SEIRA device for on-chip gas sensing using indium−tin oxide (ITO) NPs integrated with metal−organic framework (MOF) nano-composite materials for CO_2 sensing. Although the overall plasmonic enhancement factor (only 2.6×) is limited due to the low qualify-factors and strong light scattering by the randomly distributed ITO NPs, it proved a new route to extend SEIRA to gas sensing. As a key enabling material, MOF is a new type of nanoporous crystalline material consisting of metal ions and organic ligands. MOFs possess many unique material properties such as high surface area, tailorable chemistry, and tunable nanocavities, which make them very promising for gas sensing.[29−31] MOFs can also selectively adsorb certain gas molecules and concentrate them into the nanopores. By integrating MOF with plasmonic nanostructures, several groups have demonstrated new sensing devices that combine the advantages of high molecular adsorption capabilities of MOF materials and strongly localized optical field of plasmonic nanostructures, resulting in unprecedented light−matter interaction efficiencies. For example, Kreno et al. used MOF-coated nanotriangle silver antenna array for CO_2 adsorption induced refractive index (RI) sensing.[32] Sugikawa et al.[33] synthesized different noble metal NPs@MOF core−shell structures for surface-enhanced Raman scattering (SERS). However, SEIRA with high enhancement factors that can enable ultrasensitive on-chip gas sensing still remains a grand challenge.

■ RESULTS AND DISCUSSION

The proposed device is depicted in Figure 1a, consisting of a gold nanopatch array (Au-NPA) covered by a thin layer of MOF film. The whole device structure is fabricated on a Si_3N_4 nanomembrane suspended on a silicon substrate. The responses to transverse electric (TE) and transverse magnetic (TM) polarized incident light are identical due to the symmetric geometry of the plasmonic nanopatch array in the x and y directions. When light is normally irradiated onto the device, surface plasmon polaritons (SPPs) can be excited at both the Au/MOF/air and Au/Si_3N_4/air interfaces. To obtain enhanced infrared absorption for gas sensing, we prefer strong
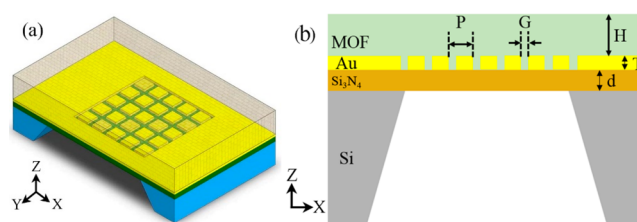

Figure 1. Schematic of (a) top and (b) cross section of the device designed in this study.

light−matter interaction between plasmonic fields with gas molecules within the entire MOF layer, rather than only enhancing small volume hot-spots around the corners of plasmonic nanoantennas that have been previously investigated by many other groups. Previous research has shown that the optical field intensity of the SPPs at metal−dielectric interfaces is related to the refractive index (RI) of the substrate materials,[34−36] i.e., lower RI will usually result in higher plasmonic field enhancement. However, plasmonic fields of the SPPs at the Au/MOF/air and Au/Si_3N_4/air interfaces become much more complex in our suspended nanomembrane device. In this paper, we will conduct an in-depth study of the SPPs at the top and bottom interfaces with respect to the thickness of the MOF and Si_3N_4 film, and reveal for the first time that the interaction between these SPPs will lead to strong cross coupling. Contrary to the fact that thick-substrate plasmonic nanostructures prefer low-index substrate for strong localized optical field, we discover a new field enhancement mechanism that nanomembrane Au-NPA achieves ultrahigh plasmonic field enhancement near the cross-coupling region of the SPPs. By engineering the coupled SPPs, we are able to achieve a high Q-factor of 203 to precisely match the vibrational band of CO_2 at 2.7 μm wavelength while still maintaining the peak transmission efficiency above 60%. Therefore, Au-NPA on Si_3N_4 nano-membrane shows exclusive advantages over plasmonic nanostructures on conventional glass substrates.[20,35]

In order to thoroughly study the SPP modes at both the Au/MOF/air and Au/Si_3N_4/air interfaces and the coupling between them, we scan the design parameters using the rigorous coupled mode analysis (RCWA) method.[37] The cross-sectional view of the device is shown in Figure 1b. The parameters that can be modified in the suspended structure are the Au-NPA periodicity P, gap G, MOF thickness H, Au thickness T, and the Si_3N_4 substrate thickness d. Among these geometry parameters, the plasmonic effect of Au NPA has been well-studied in the literature[38] and will not be discussed in this paper: the periodicity P of the Au-NPA determines the peak wavelength due to the well-known extraordinary optical transmission (EOT) effect;[39] the gap G affects the transmission intensity and also the Q-factor; and the Au thickness T also has an influence on the transmission intensity. The effective RI of the SPP modes on both interfaces are calculated using equation $\lambda_{spp} = n_{eff}P$ to understand the mechanism of the optimization. The thickness of the MOF film and the Si_3N_4 nanomembrane, on the other hand, determines the hybridization of the SPPs with the waveguide modes and, more importantly, affects the coupling between each, which has not been systematically investigated. Therefore, this paper focused on understanding the effect of the MOF thickness H and the Si_3N_4 substrate thickness d to achieve a device with ultrahigh field enhance-ment within the entire MOF layer while still maintaining high transmission intensity.
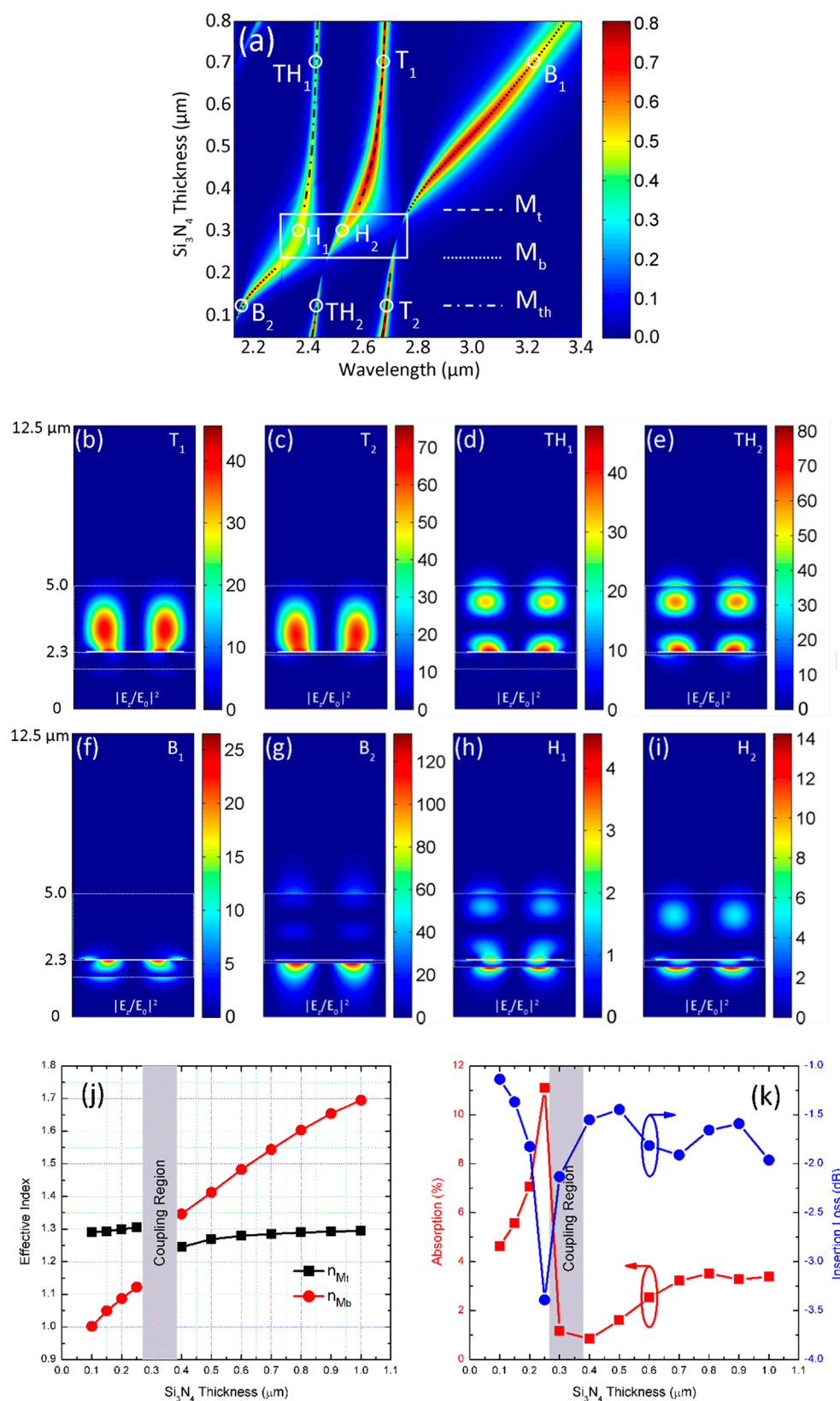
Figure 2. (a) Transmission spectra as functions of Si_3N_4 thickness with all other parameters fixed: $P = 2.08$ μm, $G = 250$ nm, $T = 40$ nm, and $H = 2.7$ μm. M_t (dash line), M_b (dot line), and M_{th} (dash dot line) represent the SPP mode at the top Au/MOF/air interface, the SPP mode at the bottom Au/Si3N4/air interface, and higher order SPP mode at Au/MOF/air interface, respectively. The white rectangle represents the cross-coupling region. The colored bar represents the transmission intensity. (b−i) Intensity of the electric field distribution of the representative points shown in (a). (j) Calculated effective index of the mode of M_t and M_b. (k) Insertion loss (transmission) and absorption as a function of the Si_3N_4 thickness. The gray region is the cross-coupling region.
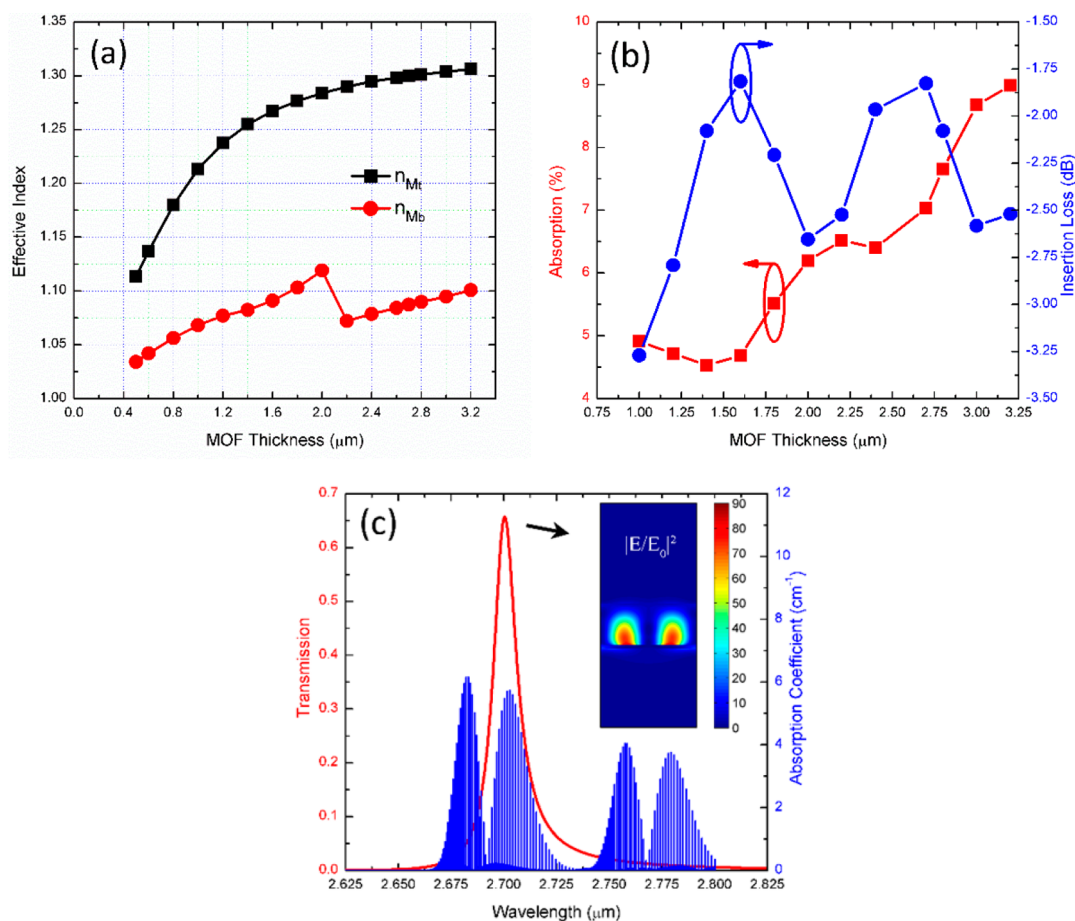
Figure 3. (a) Calculated effective index of mode M_t and M_b. (b) Insertion loss (transmission) and enhanced absorption as a function of the MOF thickness. (c) Simulated transmission spectrum of the final design (overlapped with CO_2 absorption band). The inset is the electric field distribution at the peak wavelength.

As shown in Figure 2a, there are three distinct modes in the wavelength range of interest: the SPP mode at the top Au/MOF/air interface (M_t, dash line), the SPP mode at the bottom Au/Si_3N_4/air interface (M_b, dot line), and the top SPP (M_{th}, dash dot line) which hybridizes with the high order MOF waveguide mode. The SPP mode M_t always locates around 2.7 μm with small deviation, which results in an effective index with a small variation. The intensity of the electric field distribution in Figure 2b,c clearly verified that the SPP modes are mainly localized within the MOF layer. At slightly shorter wavelength range, the top SPP mode hybridizes with the higher order waveguide mode of the MOF layer, which is marked as M_{th} in Figure 2a. Figure 2d,e represents the electric field intensity of M_{th} with a thick (TH_1) and thin (TH_2) Si_3N_4 membrane, which shows little difference in effective index. For the SPP mode M_b, when the Si_3N_4 thickness is above 400 nm, it appears at longer wavelength compared to M_t because Si_3N_3 (1.960) has a higher index than that of MOF (1.326). When the Si_3N_4 thickness is less than 250 nm, the mode M_b moves to much shorter wavelength range. This is because the effective RI of the bottom SPP is strongly influenced the thickness of the Si_3N_4 membrane. The intensity of the electric field distribution in Figure 2f,g indicates the transition from a thick membrane to a thin membrane. When the Si_3N_4 thickness is between 250 and 400 nm, however, the effective index of the top SPP M_t and the bottom SPP M_b are so close to each other that strongly coupled modes are formed. In Figure 2a, the region enclosed by the

white rectangle represents the cross-coupled mode region, where M_t and M_b cross each other. Within the rectangular region, H_1 represents the coupled mode between M_{th} and M_b, while H_2 represents the coupled mode between M_t and M_b. Clearly, the coupled modes have much lower Q-factors and the electric field intensity is very weak as shown in Figure 2h,i.

We calculate the effective index as a function of the thickness of Si_3N_4 membrane, which is shown in Figure 2j. In the coupled mode region, however, the Q-factors are low and there are no distinct transmission peaks. Therefore, the effective indices of the coupled modes are not defined. To verify the effect of SEIRA of the suspended nanostructure, an absorption coefficient $k = 1.315 \times 10^{-4}$ is added into the imaginary part of the refractive index in the MOF layer to mimic the IR absorption of CO_2. The value of the imaginary part is calculated from the HITRAN database.[40] As a comparison, the infrared absorption of pure CO_2 without any plasmonic nanostructure is also calculated, which only results in 0.174% absorption for the same optical path length. The total IR absorption and optical transmission at 2.7 μm wavelength as a function of the Si_3N_4 thickness is shown in Figure 2k. The largest IR absorption (11.5%) appears when the Si_3N_4 thickness is around 250 nm, which is close to the edge of the coupled mode region. If the Si_3N_4 membrane becomes thinner and the device enters the coupled-mode region, the IR absorption will sharply decrease. However, the insertion loss at this Si_3N_4 thickness is −3.4 dB, which increases very sharply as well. From the engineering

point of view, sufficient transmission intensity and mechanical support are also required for gas sensing. On the other hand, if the Si_3N_4 membrane becomes thicker than 380 nm, the IR absorption will first slightly increase due to the Q-factor increase. Then it will stabilize at a relatively low IR absorption. This is induced by the higher effective index of Si_3N_4, where higher intensity optical field will concentrate. This conclusion is different from Au-NPAs on thick substrates, where a low index will lead to higher plasmonic field enhancement in analogy to thinner Si_3N_4 membrane decreasing the effective RI of the bottom substrate. Thus, the optimized Si_3N_4 membrane thickness is chosen to be d = 200 nm, which takes consideration of both the plasmonic field enhancement and the optical transmission efficiency.

The thickness of the top MOF layer is another critical parameter. Thicker MOF means more adsorbed gas molecules and longer path of IR absorption. However, if the MOF layer is too thick, many more higher-order modes in the MOF layer will appear, which are very sensitive to the angular deviation of the incident light and device size.[41,42] When the incident light is not perfectly collimated or the device size is too small, the actual Q-factor will become much lower, which will reduce the field enhancement. In addition to this, thick MOF will require a much longer time to reach the equilibrium state of gas adsorption and result in slower response time.[31] Therefore, an optimized thickness is studied by scanning the MOF thickness while other parameters are fixed. As shown in Figure 3a, the effective index of mode M_b is always smaller than mode M_t when the Si_3N_4 thickness d is fixed as 200 nm. As the MOF thickness H reduces, the effective index of M_t approaches the value of air. When the MOF layer is thinner than 400 nm, mode M_t will cut off. Notably, there is a sudden change around H = 2.0 μm, which is possibly induced by the cavity effect of the MOF layer. Similarly, an imaginary part of the RI is added to MOF layer to mimic the CO_2. The IR absorption as a function of the MOF thickness is shown in Figure 3b. In this paper, the optimized MOF thickness is chosen as H = 2.7 μm after comprehensive consideration of the performance and engineering feasibility. In summary, the final parameters are chosen to be P = 2.08 μm, G = 250 nm, H = 2.7 μm, T = 40 nm, and d = 200 nm. The transmission spectrum of the final design, as well as the theoretical CO_2 absorption spectrum, is shown in Figure 3c. The inset is the electric field distribution at the peak. The decay length of the electric field is over 2.0 μm, which is much longer than the typical localized surface plasmon hotspot.

The MOF used in this device is a zeolitic imidazolate framework (ZIF-8), which has been extensively investigated due to its excellent thermal stability and selectivity toward CO_2.[43] Compared with other MOF materials that possess rough polycrystal morphologies,[29−31] the surface of ZIF-8 is relatively smooth and is suitable for thin film devices. Surface roughness was measured by the atomic force microscopy (AFM) as shown in Figure 4a, which shows a 9.8 nm roughness. Besides, due to the surface property, water molecules can only be adsorbed on the outer surface of ZIF-8 MOF, while CO_2 can diffuse into the inner pores, which makes ZIF-8 even more attractive for field sensing application.[44] The Au-NPA is fabricated by focused ion beam (FIB) etching. The scanning electron microscopy (SEM) images of the fabricated Au-NPA before and after coating MOF are shown in Figure 4b,c. As shown in the SEM image, the MOF layer fully covers the Au-NPA.
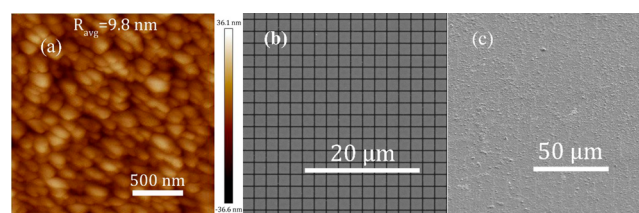

Figure 4. (a) AFM image of ZIF-8 thin film. SEM image of Au-NPA (b) before and (c) after coating the MOF thin film.

To demonstrate the functionality of the device and the enhancement provided by the hybrid plasmonic−MOF device, a quantitative CO_2 absorption measurement was performed by a Fourier transform infrared (FTIR) spectrometer. A home-made gas cell was used in the test, which has 4 mm path length (Figure S3.). One side of the gas cell is sealed by a sapphire window and the other side is sealed by the device. Different CO_2 concentrations are obtained by mixing with nitrogen (N_2) using two mass flow controllers (MFCs). The experimentally obtained transmission spectrum of the nanomembrane device normalized to the incident light is shown Figure 5a, which is broader than the simulation result. The broadening effect of the transmission spectra is mainly due to two reasons. First, the angular dependence of the incident light[45] will cause a spectrum shift and split as shown in Figure S4a. Since the light source of the commercial FTIR is not perfectly collimated as measured in Figure S4b, the transmission spectrum will be an integration of all spectra corresponding to different incident angles. Second, the fabrication imperfection will also degrade the Q-factor. For example, the slit size deviation, Au quality, and surface roughness of the MOF layer will all cause inadequate excitation of SPPs. To determine the enhancement of the device, the absorption spectra of different CO_2 concentration were collected as shown in Figure 5b. The contribution of the MOF adsorption and the plasmonic effect was determined by two reference samples: (1) MOF-coated suspended substrate without any plasmonic structure, and (2) both sides of the gas cell sealed by sapphire windows. The absorption spectra of the two references are shown in Figure 5c,d.

In order to determine the enhancement provided by the nanomembrane device, a quantitative analysis was performed by excluding the IR absorption from the 4 mm length of the gas cell. The detailed method is included in the Supporting Information and Figure S5. For the reference with two bare sapphire windows, there is no enhancement and the IR absorption is purely from CO_2 in the gas cell. The absorption coefficient α of CO_2 calculated from this reference is the actual absorption coefficient under the experimental conditions. For the nanomembrane device, the enhancement of the IR absorption comes from two effects: the gas concentration of the MOF thin film and the optical field enhancement of the plasmonic nanopatch array. For the reference device with MOF only, more CO_2 molecules were adsorbed inside the MOF layer, which essentially increases the local absorption coefficient. In addition to the concentrating effect of MOF, the plasmonic field enhancement as discussed in Figure 2 in the MOF provides an optical field enhancement effect for the integrated device. By comparing the nanomembrane device with the two reference devices, the overall enhancement factors (EFs) of the whole device and the contribution of MOF were calculated, as shown in Figure 5e. The maximum EF of the
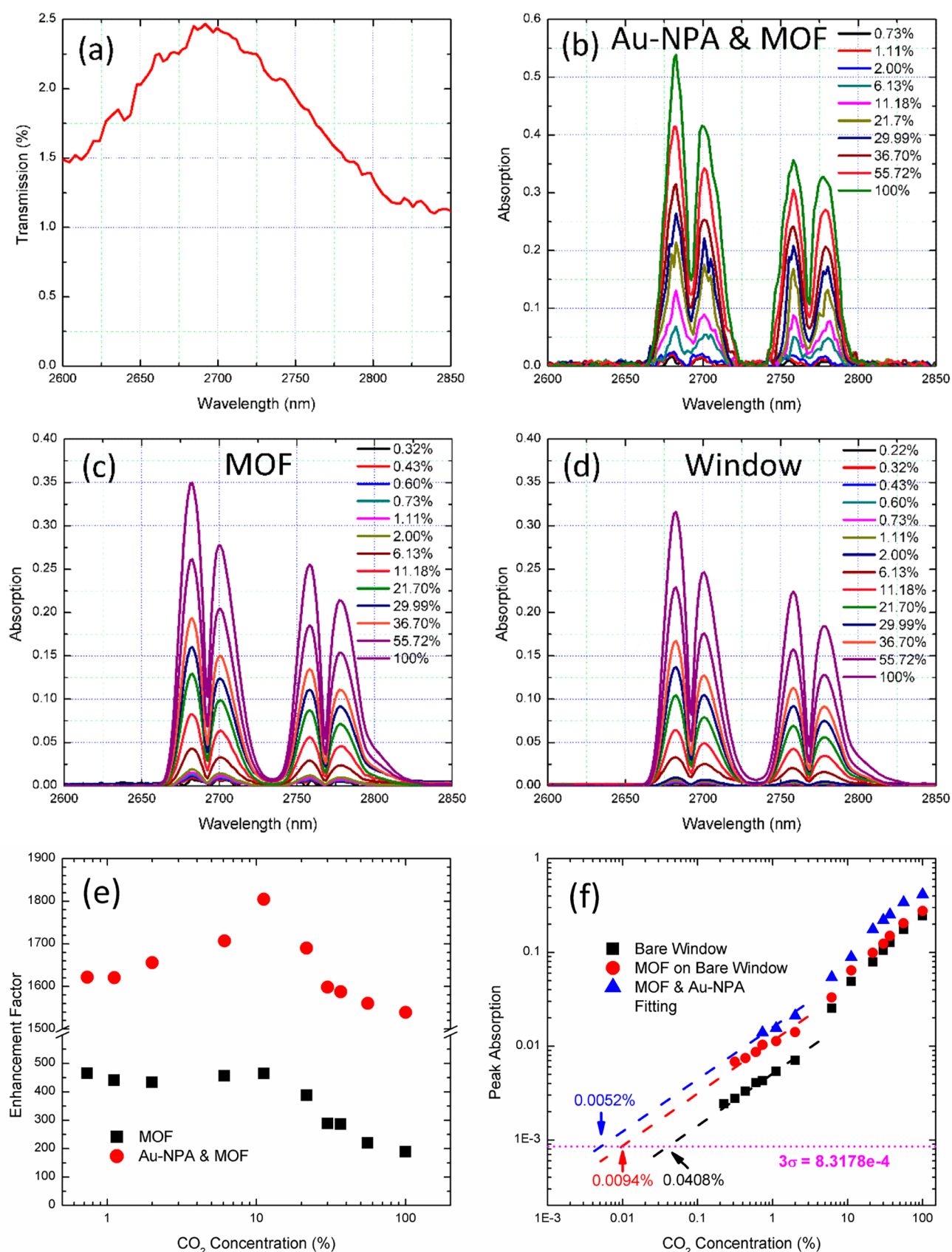
Figure 5. (a) Experimentally measured transmission spectrum by normalizing to the incident light. The absorption spectra of (b) Au-NPA coated with MOF, (c) MOF on bare window, and (d) bare window with different CO_2 concentration. (e) Calculated enhancement factor as a function of CO_2 concentration. (f) Detection limit based on noise analysis.

nanomembrane based plasmonic-MOF gas sensor is over 1800× combining both the MOF and the plasmonic nanopatch array. From the comparison of the experimental results, the maximum enhancement factor from the optical field effect of the plasmonic nanopatch array is ∼8.14, which is much smaller than the simulation results (∼38×) in Figure 2k. We mainly attribute this degradation to the low Q-factor (∼12.3) spectrum as measured in Figure 5a compared to the simulation results (∼203). Since the spectrum broadening is partially caused by the incident angle deviation of the nonperfectly collimated light source of the FT-IR, it is possible to improve the Q-factor and hence the plasmonic field enhancement factors by a mid-IR laser. In addition, as shown in Figure 5e, when the CO_2 concentration becomes lower, the SEIRA effect of the nanomembrane based device decreases. We attribute this variation to the gas molecule diffusion process that is affected by the CO_2 concentration. As the partition pressure of CO_2 decreases, it becomes increasingly difficult to push the gas molecules inside the MOF film, where the plasmonic field is the strongest at the Au NPA surface.

Figure 5f shows the peak absorption at 2682.5 nm as a function of the CO_2 concentration. We need to point out that the detection limit of our device is limited by the noise of the system. For the two reference samples (bare window and bare window with MOF film), the noise mainly comes from the noise of the white light source. For the nanomembrane plasmonic gas sensor, there is a big mismatch between the light spot size of the commercial FTIR spectrometer (∼7 mm in diameter) and the integrated device size (1 mm²). The power collected by the detector is very weak. Therefore, the dark noise from the photodetector limits the detection limit. In our measurement, the signal-to-noise ratio of the nanomembrane plasmonic gas sensor is much lower than that of the two reference devices. However, we can overcome this issue using a mid-IR laser with comparable spot size (∼1 mm²), and the detection limit will certainly be improved. In order to fairly compare the real detection limit, we use the experimentally measured noise level of the bare window device and use 3× noise levels as shown in Figure 5f for all three devices. At low CO_2 concentration, the Beer−Lambert Law is simplified to linear absorption. Therefore, the cross point of the linear fitting line of the absorption data at low concentration with the 3× noise level will be the estimated detection limit. As shown in Figure 5f, the extrapolated detection limit for 4 mm absorption path is 52, 94, and 408 ppm for the integrated device, MOF on Si_3N_4 membrane sample, and bare window sample, respectively. If the absorption path decreases, the difference of the detection limit will scale up very rapidly.

In summary, we demonstrated a suspended Si_3N_4 nanomembrane device integrating plasmonic NPAs with MOF film, which can simultaneously enhance the localized optical field and concentrate CO_2 from the ambient environment. Different than conventional SEIRA sensing relying on localized hot-spots of plasmonic nanostructures, this device operates near the coupled-mode region between the SPPs in the bottom metal/Si_3N_4 and top metal/MOF interfaces to achieve strong optical field enhancement across the entire MOF film. We successfully demonstrated on-chip gas sensing of CO_2 with more than 1800× enhancement factors within a 2.7 μm thin film by combining the contribution from the MOF gas concentration and the plasmonic field enhancement, and the detection limit was estimated to be about 52 ppm. This work proved the feasibility of developing a new type of on-chip SEIRA gas

sensing using hybrid plasmonic-MOF nanodevices with miniaturized size and ultrahigh sensitivity.

■ METHODS

Nanofabrication. The Si_3N_4 thin film was deposited onto Si wafer by atomic layer deposition method. Then Si wet etching was conducted to form the membrane structure. The Au NPA was fabricated on the 200 nm Si_3N_4 membrane via standard focused ion beam etching. The final Au NPA dimensions are nanopatch array with length L = 1830 nm, width w = 1830 nm, and thickness T = 40 nm, and periodicity $P_x = P_y$ = IP = 2080 nm.

ZIF-8 Growth. Before growing the ZIF-8 film, the substrate with Au-NPA is cleaned in piranha solution (H_2SO_4/H_2O_2, 70/30 v/v%) at 70 °C for 30 min (*Caution: Piranha solution is a very strong oxidant and is dangerous to handle without personal protective equipment; splash goggles or a face shield with safety glasses, lab coat, 18 mil neoprene gloves, chemically resistant sleeves and apron, and close toed shoes*). Then it is washed thoroughly by DI water and dried under nitrogen flow. To grow ZIF-8 thin film, the cleaned Au-NPA sample is immersed in a freshly mixed methanolic solution of 2-methylimidazole and Zn-$(NO_3)_2$ for 30 min at room temperature, followed by washing using methanol and drying under nitrogen flow. To obtain 2.7 μm MOF layer, this process is repeated 32 cycles for totally about 24 h.

Infrared Spectroscopy. The infrared absorption spectra were collected by FT-IR (Thermo Electron Nicolet 6700). Flow rates of gas were controlled by mass flow controllers (MFC) (Aalborg, GFC17) with 0−20 mL min⁻¹ flow range. Different CO_2 concentration was achieved by varying the mixing ratio of CO_2 and Ar flows.

Numerical Simulations. The simulation was performed by DiffractMOD of Rsoft photonic component design suite based on rigorous coupled-wave analysis (RCWA). In the simulation, periodic boundary condition was used to mimic the periodic array structure. To find the optimized Si_3N_4 membrane thickness and MOF thickness, the electric field in the MOF was integrated and averaged to the volume of MOF layer.

To calculate the effective index of the MOF layer and substrate, the surface plasmon resonance at the gold/MOF and gold/substrate interfaces are simulated. Then the effective index is calculated by λ_{spp} = n_{eff} · Period.

■ ASSOCIATED CONTENT

⑤ Supporting Information

The Supporting Information is available free of charge on the ACS Publications website at DOI: 10.1021/acssensors.7b00891.

> Numerical simulation of the effect of the MOF thickness; SEM and optical images of fabricated gas sensor; schematic of the experimental setup; effect of the incident angle to the transmission spectra; and the method of the data analysis (PDF)

■ AUTHOR INFORMATION

Corresponding Author

*E-mail: wang@eecs.oregonstate.edu.

ORCID

Alan X. Wang: 0000-0002-0553-498X

Notes

The authors declare no competing financial interest.

■ ACKNOWLEDGMENTS

■ REFERENCES

(1) Hartstein, A.; Kirtley, J. R.; Tsang, J. C. Enhancement of the Infrared-Absorption from Molecular Monolayers with Thin Metal Overlayers. *Phys. Rev. Lett.* **1980**, *45* (3), 201−204.

(2) Kendall, C.; Isabelle, M.; Bazant-Hegemark, F.; Hutchings, J.; Orr, L.; Babrah, J.; Baker, R.; Stone, N. Vibrational spectroscopy: a clinical tool for cancer diagnostics. *Analyst* **2009**, *134* (6), 1029−1045.

(3) Reddy, K.; Guo, Y.; Liu, J.; Lee, W.; Oo, M. K. K.; Fan, X. D. On-chip Fabry-Perot interferometric sensors for micro-gas chromatography detection. *Sens. Actuators, B* **2011**, *159* (1), 60−65.

(4) Robinson, J. T.; Chen, L.; Lipson, M. On-chip gas detection in silicon optical microcavities. *Opt. Express* **2008**, *16* (6), 4296−4301.

(5) Lai, W. C.; Chakravarty, S.; Wang, X. L.; Lin, C. Y.; Chen, R. T. On-chip methane sensing by near-IR absorption signatures in a photonic crystal slot waveguide. *Opt. Lett.* **2011**, *36* (6), 984−986.

(6) Chen, Y.; Lin, H. T.; Hu, J. J.; Li, M. Heterogeneously Integrated Silicon Photonics for the Mid-Infrared and Spectroscopic Sensing. *ACS Nano* **2014**, *8* (7), 6955−6961.

(7) Hatta, A.; Ohshima, T.; Suetaka, W. Observation of the Enhanced Infrared-Absorption of Para-Nitrobenzoate on Ag Island Films with an Atr Technique. *Appl. Phys. A: Solids Surf.* **1982**, *29* (2), 71−75.

(8) Gunde, M. K.; Kunaver, M. Infrared reflection-absorption spectra of metal-effect coatings. *Appl. Spectrosc.* **2003**, *57* (10), 1266−1272.

(9) Nishikawa, Y.; Nagasawa, T.; Fujiwara, K.; Osawa, M. Silver Island Films for Surface-Enhanced Infrared-Absorption Spectroscopy - Effect of Island Morphology on the Absorption Enhancement. *Vib. Spectrosc.* **1993**, *6* (1), 43−53.

(10) Kang, S. Y.; Jeon, I. C.; Kim, K. Infrared absorption enhancement at silver colloidal particles. *Appl. Spectrosc.* **1998**, *52* (2), 278−283.

(11) Adato, R.; Altug, H. In-situ ultra-sensitive infrared absorption spectroscopy of biomolecule interactions in real time with plasmonic nanoantennas. *Nat. Commun.* **2013**, *4*, 2154.

(12) Neuman, T.; Alonso-González, P.; Garcia-Etxarri, A.; Schnell, M.; Hillenbrand, R.; Aizpurua, J. Mapping the near fields of plasmonic nanoantennas by scattering-type scanning near-field optical microscopy. *Laser & Photonics Reviews* **2015**, *9* (6), 637−649.

(13) Neubrech, F.; Weber, D.; Lovrincic, R.; Pucci, A.; Lopes, M.; Toury, T.; de la Chapelle, M. L. Resonances of individual lithographic gold nanowires in the infrared. *Appl. Phys. Lett.* **2008**, *93* (16), 163105.

(14) Neubrech, F.; Pucci, A.; Cornelius, T. W.; Karim, S.; Garcia-Etxarri, A.; Aizpurua, J. Resonant Plasmonic and Vibrational Coupling in a Tailored Nanoantenna for Infrared Detection. *Phys. Rev. Lett.* **2008**, *101* (15), 157403.

(15) Wang, H.; Kundu, J.; Halas, N. J. Plasmonic nanoshell arrays combine surface-enhanced vibrational spectroscopies on a single substrate. *Angew. Chem., Int. Ed.* **2007**, *46* (47), 9040−9044.

(16) Huck, C.; Neubrech, F.; Vogt, J.; Toma, A.; Gerbert, D.; Katzmann, J.; Hartling, T.; Pucci, A. Surface-Enhanced Infrared Spectroscopy Using Nanometer-Sized Gaps. *ACS Nano* **2014**, *8* (5), 4908−4914.

(17) Bochterle, J.; Neubrech, F.; Nagao, T.; Pucci, A. Angstrom-Scale Distance Dependence of Antenna-Enhanced Vibrational Signals. *ACS Nano* **2012**, *6* (12), 10917−10923.

(18) Osley, E. J.; Biris, C. G.; Thompson, P. G.; Jahromi, R. R. F.; Warburton, P. A.; Panoiu, N. C. Fano Resonance Resulting from a Tunable Interaction between Molecular Vibrational Modes and a Double Continuum of a Plasmonic Metamolecule. *Phys. Rev. Lett.* **2013**, *110* (8), 087402.

(19) Nishijima, Y.; Nigorinuma, H.; Rosa, L.; Juodkazis, S. Selective enhancement of infrared absorption with metal hole arrays. *Opt. Mater. Express* **2012**, *2* (10), 1367−1377.

(20) Wang, T.; Nguyen, V. H.; Buchenauer, A.; Schnakenberg, U.; Taubner, T. Surface enhanced infrared spectroscopy with gold strip gratings. *Opt. Express* **2013**, *21* (7), 9005−9010.

(21) Srajer, J.; Schwaighofer, A.; Ramer, G.; Rotter, S.; Guenay, B.; Kriegner, A.; Knoll, W.; Lendl, B.; Nowak, C. Double-layered nanoparticle stacks for surface enhanced infrared absorption spectroscopy. *Nanoscale* **2014**, *6* (1), 127−131.

(22) Li, Y. Q.; Su, L.; Shou, C.; Yu, C. M.; Deng, J. J.; Fang, Y. Surface-enhanced molecular spectroscopy (SEMS) based on perfect-absorber metamaterials in the mid-infrared. *Sci. Rep.* **2013**, *3*, 2865.

(23) Brown, L. V.; Yang, X.; Zhao, K.; Zheng, B. Y.; Nordlander, P.; Halas, N. J. Fan-Shaped Gold Nanoantennas above Reflective Substrates for Surface-Enhanced Infrared Absorption (SEIRA). *Nano Lett.* **2015**, *15* (2), 1272−1280.

(24) Cooper, C. T.; Rodriguez, M.; Blair, S.; Shumaker-Parry, J. S. Mid-Infrared Localized Plasmons through Structural Control of Gold and Silver Nanocrescents. *J. Phys. Chem. C* **2015**, *119* (21), 11826−11832.

(25) Hoffmann, J. M.; Janssen, H.; Chigrin, D. N.; Taubner, T. Enhanced infrared spectroscopy using small-gap antennas prepared with two-step evaporation nanosphere lithography. *Opt. Express* **2014**, *22* (12), 14425−14432.

(26) Neubrech, F.; Huck, C.; Weber, K.; Pucci, A.; Giessen, H. Surface-Enhanced Infrared Spectroscopy Using Resonant Nano-antennas. *Chem. Rev.* **2017**, *117* (7), 5110−5145.

(27) Ando, M.; Kobayashi, T.; Iijima, S.; Haruta, M. Optical CO sensitivity of Au-CuO composite film by use of the plasmon absorption change. *Sens. Actuators, B* **2003**, *96* (3), 589−595.

(28) Liu, N.; Tang, M. L.; Hentschel, M.; Giessen, H.; Alivisatos, A. P. Nanoantenna-enhanced gas sensing in a single tailored nanofocus. *Nat. Mater.* **2011**, *10* (8), 631−636.

(29) Kim, K. J.; Chong, X. Y.; Kreider, P. B.; Ma, G. H.; Ohodnicki, P. R.; Baltrus, J. P.; Wang, A. X.; Chang, C. H. Plasmonics-enhanced metal-organic framework nanoporous films for highly sensitive near-infrared absorption. *J. Mater. Chem. C* **2015**, *3* (12), 2763−2767.

(30) Chong, X. Y.; Kim, K. J.; Ohodnicki, P. R.; Li, E. W.; Chang, C. H.; Wang, A. X. Ultrashort Near-Infrared Fiber-Optic Sensors for Carbon Dioxide Detection. *IEEE Sens. J.* **2015**, *15* (9), 5327−5332.

(31) Chong, X. Y.; Kim, K. J.; Li, E. W.; Zhang, Y. J.; Ohodnicki, P. R.; Chang, C. H.; Wang, A. X. Near-infrared absorption gas sensing with metal-organic framework on optical fibers. *Sens. Actuators, B* **2016**, *232*, 43−51.

(32) Kreno, L. E.; Hupp, J. T.; Van Duyne, R. P. Metal-Organic Framework Thin Film for Enhanced Localized Surface Plasmon Resonance Gas Sensing. *Anal. Chem.* **2010**, *82* (19), 8042−8046.

(33) Sugikawa, K.; Furukawa, Y.; Sada, K. SERS-Active Metal-Organic Frameworks Embedding Gold Nanorods. *Chem. Mater.* **2011**, *23* (13), 3132−3134.

(34) Valamanesh, M.; Borensztein, Y.; Langlois, C.; Lacaze, E. Substrate Effect on the Plasmon Resonance of Supported Flat Silver Nanoparticles. *J. Phys. Chem. C* **2011**, *115* (7), 2914−2922.

(35) Hoffmann, J. M.; Yin, X. H.; Richter, J.; Hartung, A.; Mass, T. W. W.; Taubner, T. Low-Cost Infrared Resonant Structures for Surface-Enhanced Infrared Absorption Spectroscopy in the Fingerprint Region from 3 to 13 mu m. *J. Phys. Chem. C* **2013**, *117* (21), 11311−11316.

(36) Huck, C.; Toma, A.; Neubrech, F.; Chirumamilla, M.; Vogt, J.; De Angelis, F.; Pucci, A. Gold Nanoantennas on a Pedestal for Plasmonic Enhancement in the Infrared. *ACS Photonics* **2015**, *2* (4), 497−505.

(37) Moharam, M. G.; Gaylord, T. K. Rigorous Coupled-Wave Analysis of Planar-Grating Diffraction. *J. Opt. Soc. Am.* **1981**, *71* (7), 811−818.

(38) Steele, J. M.; Moran, C. E.; Lee, A.; Aguirre, C. M.; Halas, N. J. Metallodielectric gratings with subwavelength slots: Optical properties. *Phys. Rev. B: Condens. Matter Mater. Phys.* **2003**, *68* (20), 205103.

(39) Ebbesen, T. W.; Lezec, H. J.; Ghaemi, H. F.; Thio, T.; Wolff, P. A. Extraordinary optical transmission through sub-wavelength hole arrays. *Nature* **1998**, *391* (6668), 667−669.

(40) Rothman, L. S.; Gordon, I. E.; Babikov, Y.; Barbe, A.; Benner, D. C.; Bernath, P. F.; Birk, M.; Bizzocchi, L.; Boudon, V.; Brown, L. R.; Campargue, A.; Chance, K.; Cohen, E. A.; Coudert, L. H.; Devi, V. M.; Drouin, B. J.; Fayt, A.; Flaud, J. M.; Gamache, R. R.; Harrison, J. J.; Hartmann, J. M.; Hill, C.; Hodges, J. T.; Jacquemart, D.; Jolly, A.; Lamouroux, J.; Le Roy, R. J.; Li, G.; Long, D. A.; Lyulin, O. M.; Mackie, C. J.; Massie, S. T.; Mikhailenko, S.; Muller, H. S. P.;

Naumenko, O. V.; Nikitin, A. V.; Orphal, J.; Perevalov, V.; Perrin, A.; Polovtseva, E. R.; Richard, C.; Smith, M. A. H.; Starikova, E.; Sung, K.; Tashkun, S.; Tennyson, J.; Toon, G. C.; Tyuterev, V. G.; Wagner, G. The HITRAN2012 molecular spectroscopic database. *J. Quant. Spectrosc. Radiat. Transfer* **2013**, *130*, 4−50.

(41) Ren, F. H.; Kim, K. Y.; Chong, X. Y.; Wang, A. X. Effect of finite metallic grating size on Rayleigh anomaly-surface plasmon polariton resonances. *Opt. Express* **2015**, *23* (22), 28868−28873.

(42) Kim, K. Y.; Chong, X. Y.; Ren, F. H.; Wang, A. X. Slow-light effect via Rayleigh anomaly and the effect of finite gratings. *Opt. Lett.* **2015**, *40* (22), 5339−5342.

(43) Fairen-Jimenez, D.; Moggach, S. A.; Wharmby, M. T.; Wright, P. A.; Parsons, S.; Duren, T. Opening the Gate: Framework Flexibility in ZIF-8 Explored by Experiments and Simulations. *J. Am. Chem. Soc.* **2011**, *133* (23), 8900−8902.

(44) Tian, F. Y.; Mosier, A. M.; Park, A.; Webster, E. R.; Cerro, A. M.; Shine, R. S.; Benz, L. Situ Measurement of CO_2 and H_2O Adsorption by ZIF-8 Films. *J. Phys. Chem. C* **2015**, *119* (27), 15248−15253.

(45) Yang, M.; Fu, Z. P.; Lin, F.; Zhu, X. Incident angle dependence of absorption enhancement in plasmonic solar cells. *Opt. Express* **2011**, *19* (14), A763−A771.